

Hydrodynamically Controlled Self-Organization in Mixtures of Active and Passive Colloids

Ian P. Madden, Linlin Wang, Juliane Simmchen,* and Erik Luijten*

Active particles are known to exhibit collective behavior and induce structure in a variety of soft-matter systems. However, many naturally occurring complex fluids are mixtures of active and passive components. The authors examine how activity induces organization in such multi-component systems. Mixtures of passive colloids and colloidal micromotors are investigated and it is observed that even a small fraction of active particles induces reorganization of the passive components in an intriguing series of phenomena. Experimental observations are combined with large-scale simulations that explicitly resolve the near- and far-field effects of the hydrodynamic flow and simultaneously accurately treat the fluid–colloid interfaces. It is demonstrated that neither conventional molecular dynamics simulations nor the reduction of hydrodynamic effects to phoretic attractions can explain the observed phenomena, which originate from the flow field that is generated by the active colloids and subsequently modified by the aggregating passive units. These findings not only offer insight into the organization of biological or synthetic active–passive mixtures, but also open avenues to controlling the behavior of passive building blocks by means of small amounts of active particles.

self-assembly. Most approaches employ nano- and microparticles as building blocks with controllable interactions to create static structures that are either in thermodynamic equilibrium or in a kinetically arrested state.^[1–6] Living systems go beyond this by operating out of equilibrium, using active components that make it possible to reach higher levels of complexity.^[7,8] Whereas collective phenomena in model systems solely comprised of active particles—either biological entities^[9–11] or self-propelled colloids^[12–17]—have been studied in great detail, the idea of organizing passive systems through the addition of active components has been far less explored. In colloidal mixtures, the active building blocks modulate the system in two ways: through the introduction of phoretic interactions that arise from concentration gradients of “propellants” and through hydrodynamic interactions the active particles generate as they

1. Introduction

There are extensive efforts in materials science, inspired by biology, to create hierarchically ordered materials through

move through the fluid. The phoretic forces refer to fluid flow resulting from the concentration gradients. These forces can drive the crystallization of passive particles, nucleating small mobile aggregates that grow into large isotropic clusters of passive building blocks centered around an active particle.^[18–20] The transport induced by hydrodynamic forces caused by the active particles moving through the fluid has been observed to organize passive colloids through segregation^[21–23] or entrainment.^[24]

In typical active systems, the propellant diffuses rapidly compared to the translation speed of the active colloid.^[18] Thus, a significant chemical gradient develops around each active particle, giving rise to a proportional fluid flow and thereby strong phoretic forces on the surrounding passive particles. Accordingly, phoretic interactions tend to dominate over hydrodynamic forces in conventionally studied systems. To explore the general situation in which both interactions are important and to study how their combination can be exploited to control dynamic colloidal aggregation, we enhance the hydrodynamic effects by extending the active particle speeds to significantly higher values. We note that natural active matter exhibits a spectrum of velocities, with some bacteria traveling up to two orders of magnitude faster^[11] than prototypical synthetic swimmers.^[18,25] An important confounding factor which tends to be ignored is that the hydrodynamic interactions are modulated once aggregation of the (active and/or passive) building blocks occurs, setting the stage for a potentially complex interplay.

I. P. Madden


Department of Materials Science and Engineering
Northwestern University
Evanston, IL 60208, USA

L. Wang, J. Simmchen

Department of Physical Chemistry
TU Dresden, Zellescher Weg 19, 01062 Dresden, Germany
E-mail: juliane.simmchen@tu-dresden.de

E. Luijten

Departments of Materials Science and Engineering
Engineering Sciences and Applied Mathematics
Chemistry
Physics and Astronomy
Northwestern University
Evanston, IL 60208, USA
E-mail: luijten@northwestern.edu

 The ORCID identification number(s) for the author(s) of this article can be found under <https://doi.org/10.1002/smll.202107023>.

© 2022 The Authors. Small published by Wiley-VCH GmbH. This is an open access article under the terms of the Creative Commons Attribution-NonCommercial License, which permits use, distribution and reproduction in any medium, provided the original work is properly cited and is not used for commercial purposes.

DOI: 10.1002/smll.202107023

We address this by fully resolved, fluctuating hydrodynamics simulations supported by experimental observations. Moreover, viewing the active units as agents that drive organization, we focus on suspensions of passive colloids to which we add a minority of self-propelled colloids.

By selecting these conditions we find that minute fractions of active components can induce large-scale anisotropic reorganization of the passive building blocks in an evolution of behaviors as the phoretic and hydrodynamic strengths are modulated during the aggregation process. The underlying mechanism of these observations turns out to be complex, with the structure of the system controlled by a combination of equilibrium and non-equilibrium interactions as well as subtle hydrodynamic effects.

2. Model

We consider a coarse-grained model of a suspension of active and passive colloids confined to a 2D plane, with parameters chosen to facilitate comparison to an experimental realization. The experimental system comprises passive SiO₂ (silica) colloids (diameter 2000 nm) in an aqueous solution of hydrogen peroxide (2.5%), to which we add Au/TiO₂ (i.e., titania with hemispherical gold coating) Janus particles (diameter 700 nm) that act as photo-active chemical “microswimmers.” Owing to density mismatch with the solution, both colloidal species settle into a single layer on the glass substrate, where we image them. Upon exposure to UV light, the Janus particles self-propel in the direction of their TiO₂ hemisphere due to photocatalysis of the hydrogen peroxide^[26] and reach a speed of $204 \pm 30 \mu\text{m s}^{-1}$ (Figure S1 and Video S1, Supporting Information). We track the trajectories of the Janus particles and observe them to travel on random paths (Figure S2, Supporting Information).

In developing a predictive model for activity-induced behavior, it is essential to separate the static (i.e., not activity-dependent) and dynamic contributions to the colloidal interactions. Through experimental determination of the pair correlation functions between the colloidal species (see Supporting Information), we establish that the static interactions can be described by expanded Lennard–Jones potentials,

$$V_{ij}(r) = \begin{cases} 4\epsilon_{ij} \left[\left(\frac{\sigma_{ij}}{r - \Delta_{ij}} \right)^{12} - \left(\frac{\sigma_{ij}}{r - \Delta_{ij}} \right)^6 \right] & r \leq r_c \\ 0 & r > r_c \end{cases} \quad (1)$$

However, even though the experimental correlation functions provide insight into the functional form of the pairwise attractions, their oscillatory behavior indicates the presence of significant many-body effects that preclude direct extraction of the well depth ϵ_{ij} . Therefore, we obtain the length scales σ_{ij} and Δ_{ij} from fits to the experimental data, and calculate the attractions using Derjaguin–Landau–Verwey–Overbeek theory,^[27,28] which captures the screened electrostatic interactions as well as the van der Waals attractions. We employ the Hamaker constants and zeta potentials for SiO₂ and Au in water ($8.4k_B T$ and -39 mV for SiO₂ and $250k_B T$ and -17 mV for Au)^[29] to calculate ϵ_{ij} .^[30] The active particles exhibit a mutual attraction of $0.4k_B T$, weak enough to be negated by their self-propulsion.

Active and passive particles experience a mutual attraction of $0.5k_B T$. Most important for our observations is the passive–passive attraction of merely $0.9k_B T$.

We develop two simulation approaches using these potentials. Following the conventional approach in the field, we first employ a strongly damped molecular dynamics (MD) simulation of active and passive colloids randomly placed on a 2D plane, with both species free to move only within the simulation plane. The solvent is implicit and propulsion of the active particles is achieved by fixing their velocity at $0.09\sigma/\tau$ (with σ the active particle diameter and τ the time unit, cf. Section 5), corresponding to the observed speed in experiment. Further details are described in Section 5. We note that the choice of an implicit solvent implies that hydrodynamic effects are neglected.

Our second approach employs a direct numerical solver to explicitly compute the full fluid flow surrounding the colloidal particles. Whereas the static pair potentials are the same as in the MD simulation, the active particle propulsion is represented by the so-called “squirmers” model,^[31] which has been shown^[32,33] to provide a good description of the flows resulting from the self-diffusion phoresis process responsible for the active particle motion.^[34] The squirmer model defines the fluid velocity around an active particle in a spherical coordinate system with respect to the Janus director \hat{e} , the axis normal to the equator separating the Janus hemispheres, which coincides with the direction of active motion. The flow field is rotationally symmetric around this axis. At the particle surface, its radial component vanishes and the field is oriented along $\hat{\theta}$, the unit vector of the polar angle θ between a point on the particle’s surface and \hat{e} . In a many-particle simulation, this flow field is imposed as a boundary condition at the surface of each active particle. We truncate the multipole expansion for the squirmer flow field at the second order and impose a relative tangential fluid velocity,

$$\mathbf{u}(\theta) = \alpha \left(\sin \theta + \frac{1}{2} \beta \sin 2\theta \right) \hat{\theta} \quad (2)$$

We set $\alpha = 0.13\sigma/\tau$, such that the particle velocity, $U = \frac{2}{3}\alpha$ (ref. [31]), has the same value as in the MD simulation and in experiment, $0.09\sigma/\tau$. The parameter β controls the stressless nature of the flow field. We vary this parameter from -5 to $+5$ (in integer increments) to achieve different swimming modes, with $\beta < 0$ realizing a so-called “pusher” (propelled through fluid flow emanating from the rear) and $\beta > 0$ resulting in a “puller” (propelled from the front).^[35] We implement this squirmer model using the smoothed profile method (SPM), a direct numerical solver for hydrodynamics that simultaneously solves the Navier–Stokes equation and the equations of motion for the immersed colloids. These equations are coupled by taking into account the forces at the fluid–colloid boundaries and the fluid–substrate interface, which are treated as diffuse interfaces^[36,37] with a no-slip boundary condition. The SPM solves the dynamics of colloidal systems more efficiently than alternative approaches to hydrodynamics by avoiding the time-consuming reconstructions of the solid–fluid boundary mesh that are required in, for example, the Lattice Boltzmann method.^[38] It also allows longer simulations than MD-based methods for hydrodynamics, such as the multi-particle collision

method,^[39–41] as it solves the Navier–Stokes equation directly and thus avoids the small time step necessary in the coarse graining of the fluid motion. Last, we incorporate phoretic interactions by imposing a $1/r^2$ force between active and passive colloids.^[19,34,42]

The physical properties of the particles are the same as in the MD simulation, but incorporation of explicit hydrodynamic flow requires a 3D simulation cell. Experimentally, we observe that the particles move above the glass substrate on a thin lubricating fluid layer.^[43] Accordingly, in the model we place the particles such that, regardless of diameter, their bottom surfaces have height $z = 2\sigma$ and we allow both species to move only in the x – y plane. This arrangement of colloids is different from the center-aligned conditions used in the MD simulations. However, it does not materially impact our conclusions because such a condition in the 2D MD simulations would only modify the relative sizes of the active and passive particles. By choosing these parameters, we ensure that the active and passive particles never directly contact the surface, but only interact with it via the intervening fluid. This lubricating layer has a thickness that varies between 1.0σ and 1.01σ (owing to the slightly corrugated nature of the surface, see Section 5). For simplicity, we confine the Janus axis of the active particle to the x – y plane and only permit it to rotate around the z -axis. Moreover, Brownian motion is imparted by random forces applied only to the colloids,^[44] by means of a generalized Langevin thermostat set to the same values as in the MD simulation. We use the same time step as in the MD simulations, but run for only 10^5 steps, since these simulations tend to be at least two orders of magnitude more costly. Details of these parameters, including the magnitude of the phoretic force, are described in Section 5.

3. Results and Discussion

3.1. Spinning Pairs

We begin with the MD model. Starting from a randomly dispersed mixture containing one active particle and ten passive particles

at a dilute particle concentration of $0.0011/\sigma^2$ ($0.0022 \mu\text{m}^{-2}$), we observe that the active colloid moves in a straight line until it collides with a passive colloid. Then, a curious spinning pair forms, where the active particle orbits the passive particle. The mean squared displacement (MSD) of the active and passive colloids in a pair (Figure 1A, blue and green curves) shows that they translate jointly. This translational motion originates from the velocity vector of the active colloid, which is not constrained to point perpendicular to the vector linking the centers of the passive colloid and the active particle. The joint motion proceeds for a few periods until impeded by a neighboring passive particle and shortly thereafter the pair falls apart. The period of rotation is 60 ms, implying a significant slow-down compared to a free active particle.

The hydrodynamic model, starting from the same initial condition, yields a markedly different result. Whenever a free active particle, either a pusher ($\beta = -5$) or a puller ($\beta = 5$), collides with a passive particle, the two particles immediately form a pair that starts spinning, but the pair no longer exhibits translational motion across the substrate (cf. orange and red MSD curves labeled “hydrodynamic” in Figure 1A). The active particle undergoes an even stronger slow-down upon being captured than in the MD simulation, with a rotational period of 100 ms. As the particles now are bottom-aligned rather than center-aligned, the orbit has decreased by a factor $\sqrt{1.4}$, implying that the particle speed has decreased even more than indicated by the change in period alone. To confirm the robustness of our observations, we repeat the hydrodynamic simulations for active particle velocities ranging from 20 – $400 \mu\text{m s}^{-1}$ and passive particle diameters of 2, 3, and $4 \mu\text{m}$. In all cases, a spinning pair form, with a rotational frequency that is lower than would be expected based upon the speed of the freely translating active particle.

Interestingly, in our comparative experiment we observe similar behavior as the active particles navigate above the cover slide and meet passive colloids. Stationary pairs form, with the active particle rotating rapidly around the center of the passive particle, as illustrated by the MSD of the active particle (Figure 1B). Upon capture, the active particle slows down to a

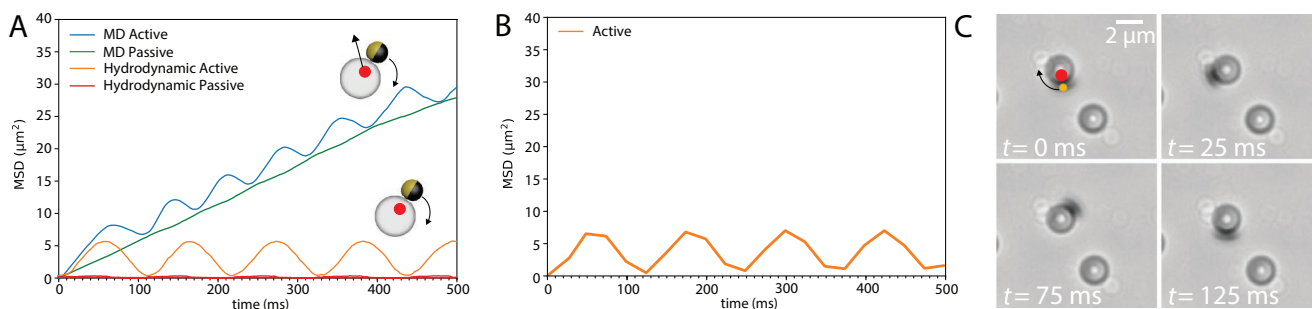


Figure 1. Formation of a spinning pair. When an active colloid encounters a passive colloid, it is “captured” and a spinning pair results. A) Mean squared displacement (MSD) obtained from two distinct computational models, along with a schematic configuration of spinning pairs. Blue and green curves show the MSD of the active and passive particle, respectively, obtained in a molecular dynamics (MD) simulation without hydrodynamic effects. In this case, the pair translates, as shown by the non-zero average slope of the MSD. Spinning takes place around the common center (red dot in upper inset; arrow indicates path of active particle), with a period of 60 ms. Orange and red curves show the MSD of the active and passive particle, respectively, when full hydrodynamic flow is included in the calculation and the active particle propagation is represented by the so-called squirmer model (cf. Section 2). After the initial stage ($t < 10$ ms) of the capture event, a stationary spinning pair results, rotating around the center of the passive particle (lower inset). Period of rotation is 100 ms. B) Experimentally determined MSD of the active particle in a spinning pair, confirming its stationary nature. Period of rotation is 125 ms. C) Micrograph time series of a spinning pair (marked in red and orange) observed in experiment.

velocity of $57 \mu\text{m s}^{-1}$, resulting in a rotational period of 125 ms (spinning micrograph time series in Figure 1C and Videos S2 and S3, Supporting Information). Similar rotating behavior has been seen in the interactions of Pt/SiO₂ Janus microparticles with fixed posts^[43] and bimetallic rods with large colloids.^[45] However, in those cases the orbital center was kept in place by geometric constraints. We attribute the discrepancy between the SPM result and the experimental period to our use of the squirmer model, which is only quantitatively correct for the flow about an isolated active particle. Although the squirmer flow should be modified when a pair is formed,^[32] we employ it here as a qualitatively sufficient representation.

It is relevant to note that in experiment the trajectories of some free active particles describe irregular rotational motion. For completeness we characterize examples of this spiraling motion in the Supporting Information. However, we emphasize that we have never observed an instance of such a particle capturing a passive and forming a spinning pair. Furthermore, our simulations do not include this tendency of active particles to describe an orbital motion, and yet display the formation of spinning pairs.

The stark contrast between the translating pair observed in the MD simulations and the stationary pair observed in the SPM calculations as well as the experiments reinforces the importance of hydrodynamic effects originating from the propulsion of the active particle. Therefore, for the remainder of this study, we exclusively employ SPM simulations in which fluctuating hydrodynamics are explicitly resolved.

This approach also helps us understand the role of the flow field in the observed behavior. A free active particle produces two pairs of counter-rotating vortices ahead and behind itself (Figure 2A, green and purple symbols, respectively). If the active particle is modeled as a pusher ($\beta < 0$) and encounters a passive particle, this passive particle will be captured (Figure 2B) in one of the anterior vortices (green symbols in Figure 2A). This then breaks the symmetry of the twinned vortex flow, and the resulting torque causes the active particle to rotate, forming the spinning pair. Conversely, if the active particle is a puller ($\beta > 0$), the direction of the flow field is reversed. This does not change the direction of motion of the active particle, but a passive particle encountered will now be trapped in one of the posterior vortices (purple symbols in Figure 2A) and be dragged along. Again the torque symmetry is broken and the pair starts to spin. Last, an active particle modeled as a “neutral swimmer” ($\beta = 0$) does not produce flow vortices and therefore can only capture passive particles through static interactions.

3.2. Ballistic Triplets

To proceed to collective phenomena in active–passive mixtures, we increase the concentration of passive particles. We observe an interesting sequence of events when a spinning pair interacts with other passive particles, provided that the active particle is modeled as a squirmer with $\beta < 0$. In this case, a passive particle encountering a spinning pair occupies the second anterior vortex and the resulting balanced triplet proceeds to

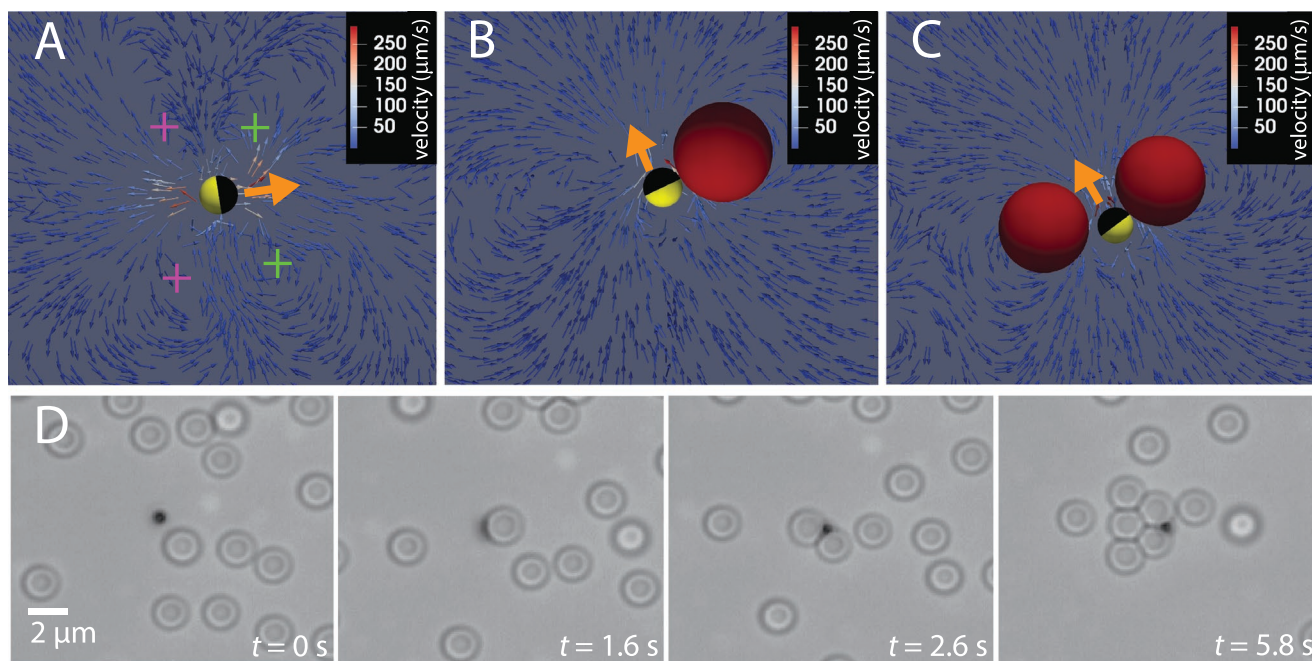


Figure 2. Initial stages of activity-induced aggregation of passive colloids. A–C) Colloidal configurations and flow fields obtained from hydrodynamics simulations. Orange arrows denote the direction of motion of the active particle. An isolated active particle, modeled as a pusher-type squirmer ($\beta = -5$), creates two vortex pairs (“+” symbols) in the fluid (A). Upon encountering a passive particle, this particle is captured in one of the two anterior vortices (green “+” symbols) and the pair starts to spin (B). A second passive particle is trapped in the second anterior vortex, the spinning is arrested, and the triplet proceeds in a linear motion (C). D) Microscopy images of an active particle forming a spinning pair with a passive particle (1.6 s), followed by the capture of a second passive particle (2.6 s), and ultimately the collection of a small “raft” (5.8 s).

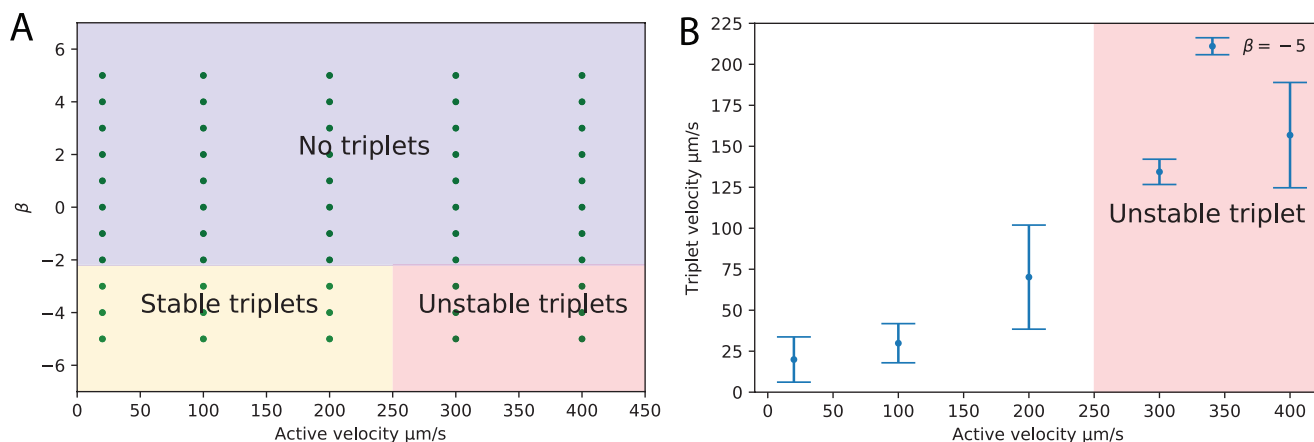


Figure 3. Triplet behavior. A) Triplet stability as a function of β and the velocity of the free active particle. Triplets only form for $\beta < -2$ and are only stable at velocities less than or equal to $200 \mu\text{m s}^{-1}$. For higher velocities, triplets form (provided that $\beta < -2$) but are short-lived. B) Average velocity of a triplet formed by an active particle with $\beta = -5$. Error bars represent the standard deviation from 25 independent simulations.

move on a ballistic trajectory without spinning (Figure 2C). For a puller-type active particle, this aggregation of a spinning pair with a second passive particle is not observed.

To examine this systematically, we vary the active particle velocity and passive diameter along with the free parameter β (Figure 3A). The formation of a stable triplet requires several conditions to be fulfilled. The active particle must be a sufficiently strong pusher ($\beta < -2$), the active particle speed should not exceed $200 \mu\text{m s}^{-1}$, and the passive particles must have a diameter that is not too large. The last condition originates from the requirement that two passive colloids must fit next to each other and remain within the vortices created by the active particle. Once a triplet has formed, its speed is considerably slower than that of a free active particle (Figure 3B).

The same phenomenon occurs in experiment. Once, owing to Brownian motion, an unbound passive particle approaches a spinning pair within a few particle diameters, it is pulled into contact and a close-packed triplet forms (Figure 2D). This aggregate of three particles immediately stops spinning and proceeds on a ballistic path (Figures S6 and S7, Supporting Information). The close match between the hydrodynamic model and the experimental observations also suggests that the Au/TiO₂ Janus colloids are described by pusher-type swimmers. Similar Janus particles were also found to be best described as pushers,^[33] supporting our choice of model parameters.

3.3. Raft Formation

Upon further increase of the concentration, ballistic triplets collide with individual passive particles. In such collisions, the free passive particle takes the place of one of the passive particles already in the triplet, and the old particle is left behind in the wake of the triplet. As a result, no larger aggregates appear. However, there is a hydrodynamic subtlety that may affect this observation. We assumed that the Janus director (i.e., squirmer axis) of each active colloid lies in the x - y plane, a simplification that is not strictly correct. Instead, hydrodynamic interactions with the surface tilt this axis slightly upward.^[46] Owing to the vicinity of the substrate, such a tilt can significantly modify

hydrodynamic flow.^[16,46–48] We first examine the effect of this tilt on an isolated active particle. Initial inspection of the 3D flow field about an active particle tilted by 5° suggests only minor changes (cf. Figure 4A,C for non-tilted and tilted, respectively). However, a projected view (Figure 4B,D for non-tilted and tilted, respectively) reveals an important consequence. The two posterior vortices (purple crosses in Figure 4B) are no longer present, but replaced by a flow that arises when the rear flow emanating from the active colloid strikes and rebounds off the substrate. This flow blocks the above-described process in which any newly encountered passive colloid causes an existing one in a triplet to fall behind.

An immediate consequence is that traveling triplets now can accumulate additional passive particles and form larger aggregates. We explicitly confirm this in longer SPM simulations (10^6 steps). Figure 4E shows a third passive colloid already added and a fourth one in the process of being captured. Evidently, phoretic forces can play a role in this as well, in particular because a reduction in speed gives rise to the build-up of larger chemical gradients. As observed elsewhere,^[18] phoresis can drive passive particles to collect isotropically around an active particle. However, in our case the aggregates remain asymmetric even when a large raft of up to 50 passive particles has formed. Considering that the phoretic field appears isotropic this far from the active particle,^[19] we view this as affirmation of the importance of the anisotropic hydrodynamic forces in raft formation.

Our experimental observations match this scenario, with the micrograph in Figure 4F displaying an arrangement nearly identical to the simulation of Figure 4E. The experiments show that the moving clusters continue to incorporate any further passive particles they encounter, resulting in the formation of far larger “rafts” in which the passive particles remain highly asymmetrically distributed around the active particle.

3.4. Merging Rafts

Last, we examine the interaction between multiple rafts. Here, in a simulation of 15 passive particles and three active particles,

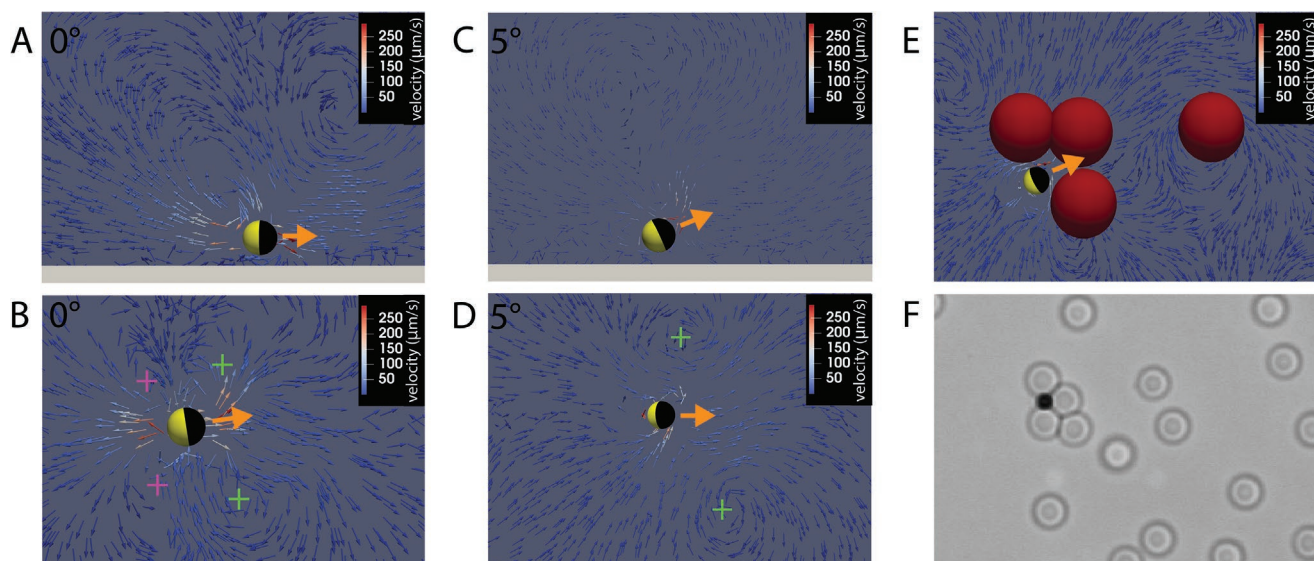


Figure 4. Effect of active particle tilt on the surrounding hydrodynamic flow field. A,B) Side and top view of the flow field around a squirmer-type ($\beta = -5$) active particle with its Janus axis (orange vector) in the x - y plane, that is, 0° tilt. The top view (B) illustrates the anterior (green) and posterior (purple) vortex pairs. This flow field does not result in arrangements larger than a triplet of one active and two passive particles. C,D) Side and top view of the flow field around the same particle, but now with an upward tilt of 5° . The two trailing vortices are no longer present. E) Formation of a small raft with more than two passive colloids, held together by the flow field and phoretic forces from a tilted active particle. F) Experimental image showing an arrangement closely resembling the simulation configuration of panel (E).

three rafts are colored red, green, and yellow (Figure 5A). The green and yellow rafts merge into one entity while the red raft continues to grow. The resulting composite raft is stationary but continues to feature internal rearrangements. Eventually these dynamics lead to the raft's dissolution. This “living crystal” behavior is typical in active matter, observed in purely active systems^[12] as well as mixtures of active and passive colloids.^[18–24,49,50] As a testament to the robustness of our computational model, similar growth and merging events are observed in experiment, continuing to arrangements that go well beyond the sizes that—due to computational constraints—can be attained in the simulations. Starting from a triplet configuration, a third passive particle usually occupies the space between the first two, whereas capturing of a fourth particle results in a rhomboid structure. Eventually, a raft of 20 or more colloids assembles (Videos S4 and S5, Supporting Information). Once two larger rafts have formed, we observe their collision and merging (Figure 5B; Video S7, Supporting Information). In this process, the outer particle layers of both rafts adjust to create a single closely packed arrangement. This merged raft can be either static, if the propulsion induced by different active particles happens to cancel out, or dynamic, that is, slowly moving or rotating. Internal rearrangements during the merging process may cause pieces to break off, and collisions with additional active particles or with smaller rafts may either result in growing the raft or cause it to dissolve completely. We emphasize that the (isotropic) static passive–passive interactions are too weak to drive this aggregation; it is induced by the motion of a single active particle. We further corroborate this by turning off the UV exposure. This instantaneously halts the motion of the active particle and the raft begins to disassemble (Video S6, Supporting Information).

4. Conclusion

We have explored aggregation and self-organization in mixtures of passive colloids and a minority of self-propelled particles. Activity-driven emergent organization has been observed in a variety of biological and synthetic systems, for example, flow-induced crystallization of colloids,^[12,21–24] spontaneous active liquid crystal ordering,^[10,51] and the realization of various forms of dynamic collective behavior in metal–dielectric Janus particles^[13,18–20] and self-propelled emulsion droplets.^[16] However, the role of hydrodynamic and phoretic effects in producing structures and patterns is generally not well established. A key bottleneck is that the hydrodynamic flow fields are modulated by the very patterns that they produce, resulting in a costly and complex computational problem. We have addressed the role of hydrodynamics for a prototypical model system, using large-scale computational modeling tightly coupled with experimental observations. We demonstrated that a small minority component of active colloids can organize an ensemble of passive Brownian colloids into complex, dynamic arrangements. These aggregates exhibit an anisotropy explicitly controlled by the interplay of the hydrodynamic flow field originating from the “pusher” nature of the active particles, the tilt of the propulsion axis, and phoretic forces. These mechanistic insights are afforded by simulations that dynamically resolve the configuration-dependent flow field and employ it to evolve the colloidal motion.

By illustrating that hydrodynamic forces induced by active components go well beyond the phoretic forces that are typically invoked, our findings imply that dispersions of passive and active components can be manipulated by tuning the dynamic force fields created by the active particles. Moreover, our approach and findings may provide insight into biological systems comprised of active and passive components.

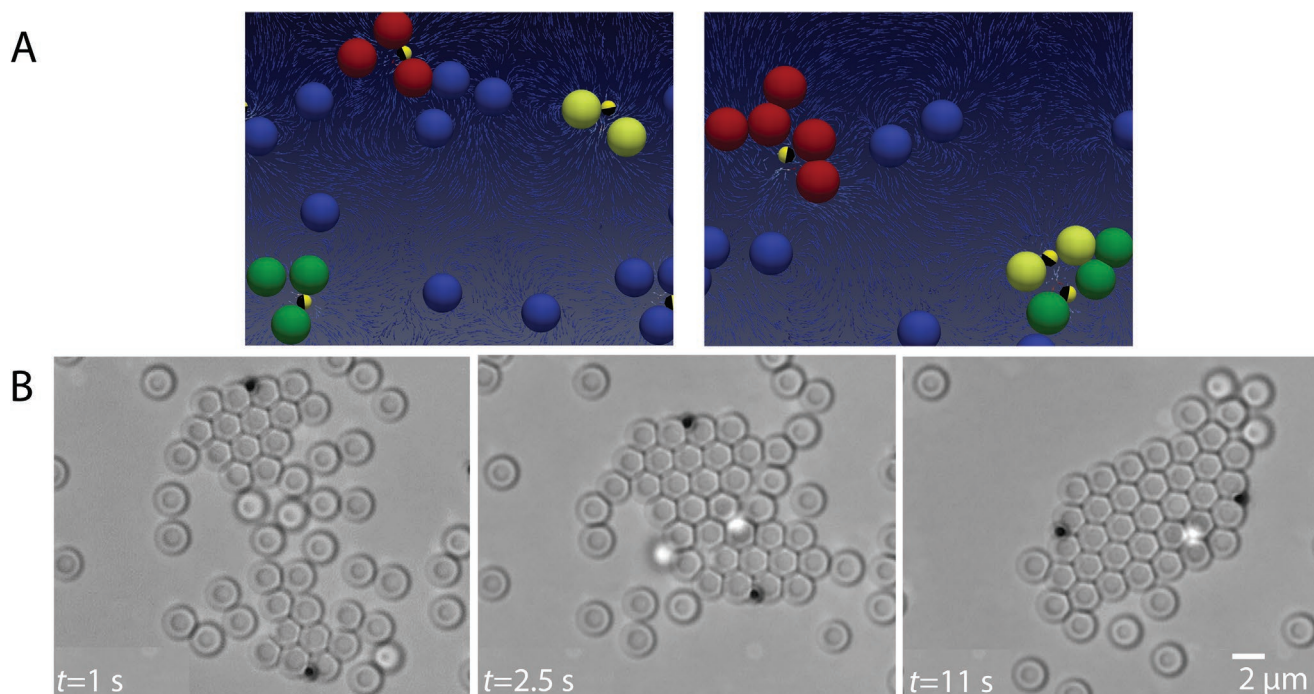


Figure 5. Raft merging events. A) Simulations of a merging event of two rafts, colored yellow and green, in the presence of a third raft (red). Some particles appear twice owing to periodic boundary conditions. The time elapsed between the two panels corresponds to 1210τ or 0.36 s. B) Optical micrographs showing the merging process of extended rafts.

5. Experimental Section

Molecular Dynamics Simulations: The MD simulations were performed with the LAMMPS MD package, using a 2D simulation cell with lateral dimensions $100 \times 100\sigma^2$. Periodic boundary conditions were applied in the x - and y -directions. The unit length σ corresponded to the diameter of an active particle (700 nm). Accordingly, the passive particles had a diameter $\sigma_p = 2.857\sigma$. The active particle mass was taken as the unit mass $m = 7.597 \times 10^{-16}$ kg, based solely on the density of titania, 4.23 g cm^{-3} (the mass of the 30-nm-thick gold-coated hemispherical shell was neglected). Passive silica particles had a mass density of 2.65 g cm^{-3} and were thus 14.6 times more massive. Both species experienced Brownian motion and hydrodynamic drag, which were imposed through a Langevin thermostat. The dynamic viscosity of water at 20°C is $\eta = 1.002 \times 10^{-3} \text{ kg (m} \times \text{s)}^{-1}$. Adopting the thermal energy $k_B T$ as the energy scale, a unit time $\tau = \sqrt{m\sigma^2/\epsilon} = 300.8 \times 10^{-6} \text{ s}$ was obtained. Thus, in reduced units the viscosity was $277.7m/(\sigma\tau)$ and the drag was $\gamma = 3\pi\eta\sigma = 2.617 \times 10^3 m/\tau$ on the active particles and $\gamma_p = 3\pi\eta\sigma_p = 7.478 \times 10^3 m/\tau$ on the passive particles. Accordingly, the damping times (ratio of particle mass and drag) were $3.82 \times 10^{-4}\tau$ and $1.95 \times 10^{-3}\tau$, respectively. The reduced temperature was $T = 1.0$. For all potentials a cutoff $r_c = 10\sigma$ was chosen and the potentials were shifted such that $V_j(r_c) = 0$. A time step of 0.01 τ was employed. The total run time of the spinning simulation was 10^6 steps, with samples taken every 100 steps.

Hydrodynamic Simulations: The hydrodynamic simulations were performed using the SPM method implemented in the KAPSEL simulation software.^[38] The interaction potentials (described in the main text), particle masses and dimensions, and temperature were all identical to those in the MD simulations. The viscosity was set to the same value as well, but in the SPM method was imposed via the fluid properties. The simulations proceeded with the same time step, but unlike the MD simulation employed a cubic, periodically replicated domain. In the spinning simulations, the domain had a linear size of 25.6σ , whereas all other SPM calculations used a linear size of 51.2σ to minimize periodic boundary effects. This domain was subdivided into cubic cells with linear size 0.2σ for the application of the SPM method. The microscope

slide that constituted the substrate in the experiments was represented by a surface of overlapping immobile colloids with diameter σ that were spaced 0.2σ apart on a square grid and placed at a height $z = 0.5\sigma$. The spherical particle class in KAPSEL was modified to support the simulation of binary mixtures (i.e., active and passive particles). Each colloid in the SPM treatment had a diffuse interface representing a smooth transition from the fluid to the particle. The width of this interface was fixed to extend 0.2σ beyond the colloid surface. For the active particles, the velocity boundary condition defined by the squirmer model, Equation (2), was imposed in this interfacial region. KAPSEL's translation and rotation update procedure was also modified such that the active and passive colloids translated only in the x - y plane and the Janus director of each active colloid could rotate only around the z -axis. The Navier–Stokes equation was solved using a linear interpolation scheme, with the velocity correction coefficient and rotational correction coefficient both set to 1.0. The slip tolerance, measured between the colloid surface and the surface fluid slip velocity, was set to $0.001\sigma/\tau$. If this tolerance was exceeded, a maximum of 100 iterative solutions were performed with the Navier–Stokes solver. In each iterations the surface fluid slip velocity would be updated and the Navier–Stokes equations resolved for slip convergence. The proportionality constant κ for the phoretic force κ/r^2 was obtained by observing in experiment that active colloids will only aggregate up to five layers of passive particles (Video S4, Supporting Information), and therefore it was reasoned that the phoretic attraction decays to $\mathcal{O}(k_B T)$ over a range of $10 \mu\text{m}$. Thus, κ was set to $14.285\epsilon\sigma$.

Chemicals: All chemicals were bought and used without further purification: titanium (IV) isopropoxide TTIP (Alfa Aesar Co. Ltd.); dodecylamine DDA (Fluka); formic acid (Sigma-Aldrich); potassium chloride (VWR); hydrogen peroxide 30% H_2O_2 (Sigma-Aldrich); $2 \mu\text{m}$ silica particles (Sigma-Aldrich). Solvents (methanol, acetonitrile, and ethanol) were used in analytical grade without any additional treatment.

Synthesis of Au/TiO₂ Microparticles: The procedure described in ref. [52] was followed. 180 μL distilled water was added to a mixture of 45 mL acetonitrile and 110 mL methanol. After adding 280 mg DDA, the solution was stirred for 10 min. Subsequently, 1 mL TTIP was added within 5 min and the solution was stirred at room temperature for 72 h. The resulting

suspension was centrifuged at 2000 rpm for 2.5 min and the precipitate was washed three times with 15 mL methanol and then dried for 3 h at 80 °C. The particles were subsequently calcinated at 600 °C for 2 h under nitrogen atmosphere. The particles were deposited in a monolayer using a Langmuir–Blodgett trough and monolayers of calcined TiO₂ particles were coated with a thin (30 nm) gold layer using thermal deposition.

Microscopic Analysis: All experiments were performed using an inverted optical microscope (Carl Zeiss Microscopy GmbH, Germany) equipped with a Zeiss Colibri lamp. The UV LED (385 nm) was used as illumination for photocatalytic propulsion. The power of the UV lamp was 315 mW, as specified by Zeiss. Using a Gentec Uno Powermeter connected to a PH100-SiUV-Do sensor it was determined that after passing the internal optics 1.9 mW UV light reached the sample. In a typical experiment of a mixture of active and passive particles, different amounts of active particles in deionized (DI) water were mixed with passive silica particles in DI water and the required volume of H₂O₂ solution was added to reach a desired concentration (0.05–5.0%). Videos were recorded with a Zeiss camera (Axiocam 702 Mono) at a frame rate of 40 fps. A precise analysis of the trajectories was performed using ImageJ.

Experiments for Pair Potentials: Individual particle species (SiO₂, TiO₂, Au) were dispersed in DI water, containing low percentages of H₂O₂ ranging from 0% to 2.5%. Short video sequences were recorded under different illumination conditions, ranging from 0% UV light to 100% UV light using a Zeiss camera (Axiocam 702 Mono) at a frame rate of 40 fps.

Supporting Information

Supporting Information is available from the Wiley Online Library or from the author.

Acknowledgements

This work was supported by the Center for Bio-Inspired Energy Science, an Energy Frontier Research Center funded by the U.S. Department of Energy, Office of Science, Basic Energy Sciences (BES), under Award DE-SC0000989. The authors thank R. Yamamoto and J. Molina for kind assistance with the KAPSEL software that implements the SPM, specifically in aiding us to modify the software for the purposes of this manuscript. The authors thank the Quest high-performance computing facility at Northwestern University for computational resources. J.S. acknowledges Freigeist grant number 91619 from the Volkswagen Foundation and the Fulbright–Cottrell Foundation. L.W. acknowledges financial support from the China Scholarship Council. The authors thank T. Gemming for access to electron microscopy and S. Heckel for taking images of active–passive mixtures.

Conflict of Interest

The authors declare no conflict of interest.

Data Availability Statement

The data that support the findings of this study are available in the supplementary material of this article.

Keywords

active particles, aggregation, colloids, hydrodynamics, Janus micromotors, simulations

Received: November 14, 2021

Revised: February 4, 2022

Published online: March 19, 2022

- [1] B. Gates, Y. Xia, *Adv. Mater.* **2001**, *13*, 1605.
- [2] J. D. Hartgerink, E. Beniash, S. I. Stupp, *Science* **2001**, *294*, 1684.
- [3] D. H. Gracias, V. Kavthekar, J. C. Love, K. E. Paul, G. M. Whitesides, *Adv. Mater.* **2002**, *14*, 235.
- [4] Z. Zhang, S. C. Glotzer, *Nano Lett.* **2004**, *4*, 1407.
- [5] A. M. Kalsin, M. Fialkowski, M. Paszewski, S. K. Smoukov, K. J. M. Bishop, B. A. Grzybowski, *Science* **2006**, *312*, 420.
- [6] A. Aliprandi, M. Mauro, L. De Cola, *Nat. Chem.* **2016**, *8*, 10.
- [7] M. C. Marchetti, J. F. Joanny, S. Ramaswamy, T. B. Liverpool, J. Prost, M. Rao, R. A. Simha, *Rev. Mod. Phys.* **2013**, *85*, 1143.
- [8] D. Needleman, Z. Dogic, *Nat. Rev. Mater.* **2017**, *2*, 17048.
- [9] J.-F. Joanny, S. Ramaswamy, *Nature* **2010**, *467*, 33.
- [10] T. Sanchez, D. T. N. Chen, S. J. DeCamp, M. Heymann, Z. Dogic, *Nature* **2012**, *491*, 431.
- [11] A. P. Petroff, X.-L. Wu, A. Libchaber, *Phys. Rev. Lett.* **2015**, *114*, 158102.
- [12] J. Palacci, S. Sacanna, A. P. Steinberg, D. J. Pine, P. M. Chaikin, *Science* **2013**, *339*, 936.
- [13] J. Yan, M. Han, J. Zhang, C. Xu, E. Luijten, S. Granick, *Nat. Mater.* **2016**, *15*, 1095.
- [14] J. Zhang, E. Luijten, B. A. Grzybowski, S. Granick, *Chem. Soc. Rev.* **2017**, *46*, 5551.
- [15] S. A. Mallory, C. Valeriani, A. Cacciuto, *Annu. Rev. Phys. Chem.* **2018**, *69*, 59.
- [16] S. Thutupalli, D. Geyer, R. Singh, R. Adhikari, H. A. Stone, *Proc. Natl. Acad. Sci. U. S. A.* **2018**, *115*, 5403.
- [17] A. Aubret, M. Youssef, S. Sacanna, J. Palacci, *Nat. Phys.* **2018**, *14*, 1114.
- [18] D. P. Singh, U. Choudhury, P. Fischer, A. G. Mark, *Adv. Mater.* **2017**, *29*, 1701328.
- [19] J. Stürmer, M. Seyrich, H. Stark, *J. Chem. Phys.* **2019**, *150*, 214901.
- [20] F. Hauke, H. Löwen, B. Liebchen, *J. Chem. Phys.* **2020**, *152*, 014903.
- [21] S. Li, H. Jiang, Z. Hou, *Soft Matter* **2015**, *11*, 5812.
- [22] A. V. Singh, V. Kishore, G. Santomauro, O. Yasa, J. Bill, M. Sitti, *Langmuir* **2020**, *36*, 5435.
- [23] H. R. Vutukuri, M. Lisicki, E. Lauga, J. Vermant, *Nat. Commun.* **2020**, *11*, 2628.
- [24] R. C. Krafnick, A. E. García, *Phys. Rev. E* **2015**, *91*, 022308.
- [25] W. F. Paxton, A. Sen, T. E. Mallouk, *Chem. - Eur. J.* **2005**, *11*, 6462.
- [26] R. Dong, Q. Zhang, W. Gao, A. Pei, B. Ren, *ACS Nano* **2016**, *10*, 839.
- [27] B. V. Derjaguin, L. Landau, *Acta Physicochim. USSR* **1941**, *14*, 633.
- [28] E. J. Verwey, J. T. G. Overbeek, *Theory of the Stability of Lyophobic Colloids*, Elsevier, Amsterdam **1948**.
- [29] H. D. Ackler, R. H. French, Y.-M. Chiang, *J. Colloid Interface Sci.* **1996**, *179*, 460.
- [30] E. C. Donaldson, W. Alam, in *Wettability* (Eds: E. C. Donaldson, W. Alam), Gulf Publishing Company, Houston, Texas **2008**, pp. 57–119.
- [31] J. R. Blake, *J. Fluid Mech.* **1971**, *46*, 199.
- [32] M. N. Popescu, W. E. Uspal, Z. Eskandari, M. Tasinkevych, S. Dietrich, *Eur. Phys. J. E: Soft Matter Biol. Phys.* **2018**, *41*, 145.
- [33] A. I. Campbell, S. J. Ebbens, P. Illien, R. Golestanian, *Nat. Commun.* **2019**, *10*, 3952.
- [34] J. L. Anderson, *Annu. Rev. Fluid Mech.* **1989**, *21*, 61.
- [35] M. T. Downton, H. Stark, *J. Phys.: Condens. Matter* **2009**, *21*, 204101.
- [36] J. J. Molina, Y. Nakayama, R. Yamamoto, *Soft Matter* **2013**, *9*, 4923.
- [37] Y. Nakayama, R. Yamamoto, *Phys. Rev. E* **2005**, *71*, 036707.
- [38] R. Yamamoto, K. Kim, Y. Nakayama, K. Miyazaki, D. R. Reichman, *J. Phys. Soc. Jpn.* **2008**, *77*, 084804.
- [39] A. Malevanets, R. Kapral, *J. Chem. Phys.* **1999**, *110*, 8605.
- [40] G. Gompper, T. Ihle, D. M. Kroll, R. G. Winkler, *Advanced Computer Simulation Approaches for Soft Matter Sciences III*, Vol. 221, Advances in Polymer Science, Springer, Berlin **2008**, pp. 1–87.
- [41] J. K. Whitmer, E. Luijten, *J. Phys.: Condens. Matter* **2010**, *22*, 104106.
- [42] M.-J. Huang, J. Schofield, R. Kapral, *New J. Phys.* **2017**, *19*, 125003.

- [43] J. Simmchen, J. Katuri, W. E. Uspal, M. N. Popescu, M. Tasinkevych, S. Sánchez, *Nat. Commun.* **2016**, *7*, 10598.
- [44] T. Iwashita, Y. Nakayama, R. Yamamoto, *J. Phys. Soc. Jpn.* **2008**, *77*, 074007.
- [45] D. Takagi, J. Palacci, A. B. Braunschweig, M. J. Shelley, J. Zhang, *Soft Matter* **2013**, *10*, 1784.
- [46] W. E. Uspal, M. N. Popescu, S. Dietrich, M. Tasinkevych, *Soft Matter* **2015**, *11*, 434.
- [47] S. Das, A. Garg, A. I. Campbell, J. Howse, A. Sen, D. Velegol, R. Golestanian, S. J. Ebbens, *Nat. Commun.* **2015**, *6*, 8999.
- [48] A. Leeth Holterhoff, M. Li, J. G. Gibbs, *J. Phys. Chem. Lett.* **2018**, *9*, 5023.
- [49] F. Kümmel, P. Shabestari, C. Lozano, G. Volpe, C. Bechinger, *Soft Matter* **2015**, *11*, 6187.
- [50] S. Ramanarivo, E. Ducrot, J. Palacci, *Nat. Commun.* **2019**, *10*, 3380.
- [51] V. Schaller, C. Weber, C. Semmrich, E. Frey, A. R. Bausch, *Nature* **2010**, *467*, 73.
- [52] S. Tanaka, D. Nogami, N. Tsuda, Y. Miyake, *J. Colloid Interface Sci.* **2009**, *334*, 188.